Research Square

Preprints are preliminary reports that have not undergone peer review.
They should not be considered conclusive, used to inform clinical practice,
or referenced by the media as validated information.

FOXM1 inhibition primes terminal differentiation of human iPSC-derived hepatocytes

Mayana Zatz

mayazatz@usp.br

University of São Paulo

Kayque Alves Telles-Silva

University of São Paulo https://orcid.org/0000-0002-2994-609X

Lara Pacheco

University of São Paulo

Sabrina Komatsu

University of São Paulo

Fernanda Chianca

University of São Paulo

Gustavo Chagas

University of São Paulo

Gabrielly Cristine Martins

Federal University of São Paulo

Maria Gridina

The Federal Research Center

Daria Panchenko

Sirius University for Science and Technology

Valdemir Melechco Carvalho

Fleury Group

Elia G. Caldini

Medical School of the University of São Paulo

Veniamin S. Fishman

Sirius University for Science and Technology

Michelle Arkin

University of California at San Francisco https://orcid.org/0000-0002-9366-6770

Ernesto Goulart

University of São Paulo

Article

Keywords: liver, human iPSCs, hepatocytes, FOXM1, TOP2A, polyploidization

Posted Date: December 10th, 2025

DOI: https://doi.org/10.21203/rs.3.rs-7594791/v1

License: This work is licensed under a Creative Commons Attribution 4.0 International License.
Read Full License

Additional Declarations: There is no duality of interest

Version of Record: A version of this preprint was published at Cell Death Discovery on July 8th, 2026.
See the published version at https://doi.org/10.1038/s41420-026-03178-9.

FOXM1 inhibition primes terminal differentiation of human iPSC-derived hepatocytes

Kayque Alves Telles-Silva, Lara Pacheco, Sabrina Komatsu, Fernanda Chianca, Gustavo Chagas, Gabrielly Cristine Martins, Maria Gridina, Daria Panchenko, Valdemir Melechco Carvalho, Elia G. Caldini, Veniamin S. Fishman, Michelle Arkin, Ernesto Goulart*, Mayana Zatz*.

***=Authors co-supervised this work**

Authors and Affiliations

Human Genome and Stem-Cell Research Center (HUG-CEL), Department of Genetics and Evolutionary Biology, Institute of Biosciences, University of São Paulo, São Paulo, SP, Brazil

Kayque Alves Telles-Silva, Lara Pacheco, Sabrina Komatsu, Fernanda Chianca, Gustavo Chagas, Ernesto Goulart, Mayana Zatz.

Department of Pharmaceutical Chemistry, University of California, San Francisco, San Francisco, CA, USA

Kayque Alves Telles-Silva & Michelle Arkin.

Department of Hematology and Oncology, Federal University of São Paulo, São Paulo, SP, Brazil

Gabrielly Cristine Martins.

The Federal Research Center Institute of Cytology and Genetics, Novosibirsk, Russia

Maria Gridina & Veniamin S. Fishman.

Sirius University for Science and Technology, Sochi, Russia

Daria Panchenko & Veniamin S. Fishman.

Division of Research and Development, Fleury Group, São Paulo, Brazil

Valdemir Melechco Carvalho.

Laboratory of Cellular Biology, Department of Pathology, Medical School, University of São Paulo, São Paulo, SP, Brazil

Elia G. Caldini.

Corresponding author: Mayana Zatz, mayazatz@usp.br.

Keywords: liver, human iPSCs, hepatocytes, FOXM1, TOP2A, polyploidization.

Word count: 2,702 words (excluding abstract, materials & methods, references, figures and tables).

Number of figures and tables: 5 (five) main figures, 1 (one) graphical abstract figure, 3 (three) supplementary figures, and 4 (four) supplementary tables.

ABSTRACT

Human iPSC-derived hepatocytes are widely used in disease modeling. However, late embryonic development in the human liver remains elusive, which hinders differentiation.

During late liver embryonic development, Topoisomerase II (TOP2) is downregulated; however, its role in differentiation is unclear. We replicated the TOP2 silencing at birth and identified a transcription factor crucial for hepatocyte differentiation in vitro. Subtoxic inhibition of TOP2 reduces nuclear chromatin condensation without causing DNA damage. RNA-seq analysis revealed that TOP2 inhibition induced cell cycle arrest, accompanied by FOXM1 downregulation. ATAC-seq confirmed that TOP2A inhibition decreased chromatin accessibility and modulated the Wnt/β-catenin pathway. Proteomic analysis demonstrated that FOXM1 inhibition mimicked TOP2A-mediated cell cycle arrest and reduced the levels of fetal hepatocyte proteins. Prolonged FOXM1 inhibition results in increased hepatocyte polyploidization, enhanced CYP450 activity, and improved lipid metabolism. Our findings suggest that FOXM1 inhibition promotes terminal differentiation of human iPSC-derived hepatocytes, potentially paving the way for understanding late embryonic development in the human liver.

INTRODUCTION

Human induced pluripotent stem cells (iPSCs) have emerged as a tool to bridge developmental biology, regenerative medicine, and disease modeling because of their capacity to differentiate into various cell types, including hepatocytes (1). The need for a viable hepatocyte source for drug testing has driven the development of new techniques for hepatic differentiation (2). Hepatocyte differentiation from iPSCs requires specific factors (Wnt3a, Activin A, HGF) and signaling pathways that control cell proliferation and maturation (3). iPSC-derived hepatocytes show a fetal-like phenotype; thus, they are frequently named hepatocyte-like cells (HLCs), with a proliferative profile and lack of mature metabolism compared to primary human hepatocytes

(PHHs) (4). Therefore, no protocol has achieved terminal differentiation of iPSCs into hepatocytes using tridimensional, coculture-based, organoid, or microfluidic platforms (5).

Topoisomerases resolve DNA structures and TOP2 is crucial for DNA replication during embryogenesis (6). TOP2 regulates hepatocyte proliferation (7). Among the TOP2A and TOP2B isoforms, TOP2A upregulation facilitates oncogenesis by enhancing cellular proliferation (8). TOP2A downregulation after weaning coincides with hepatocyte terminal maturation when the liver metabolism changes (9), revealing TOP2A's role in liver development (10). TOP2A and FOXM1 are frequently associated with hepatocyte proliferation studies (11, 12). FOXM1 regulates cell cycle progression and TOP2A expression during embryogenesis and cancer development (13). The TOP2-FOXM1 interaction maintains a balance between stemness and lineage commitment (14). During late embryonic development, liver parenchymal cells stop proliferating and significantly increase their functionality, especially hepatocyte polyploidization, which is crucial for liver homeostasis (15). Foxm1-deficient mice exhibit reduced hepatocyte mitosis and polyploidy (16), suggesting that FOXM1 may be involved in the regulation of hepatocyte cell cycle and polyploidization. However, the TOP2-FOXM1 axis has not been explored in the context of hepatocyte terminal differentiation.

In this study, we investigated the effects of TOP2 and FOXM1 on the differentiation of human iPSC-derived hepatocytes. FOXM1 inhibition promotes hepatocyte maturation, including cell cycle arrest and polyploidy. FOXM1 suppression reduces fetal markers while increasing adult hepatic gene expression by modulating the Wnt/β-catenin pathway. TOP2A functions as an integral partner of this network.

RESULTS

Subtoxic Etoposide Treatment Promotes Quiescence of HLCs

To assess the effect of etoposide on TOP2 inhibition in HLCs, human iPSCs were differentiated into HLCs (Supplementary Fig. S1A). The HLCs exhibited hepatocyte morphology on day 20 (Supplementary Fig. S1B) and more than 71.4% double-positive staining for ALB and UGT1A1 (Supplementary Fig. S1C) and significant hepatocyte-specific gene expression (*HNF4A*, *ALB*, and *CYP3A4*) (Supplementary Fig. S1D). To determine its subtoxic concentrations, we exposed HLCs to etoposide for five days (Fig. 1A). Etoposide did not induce apoptosis at concentrations of up to 3 mM, with similar responses observed in HLCs and HepG2 cells. (Fig. 1B). We also validated apoptosis using teniposide, which is nontoxic at low concentrations (Fig. 1C). Therefore, 10 μM of etoposide was selected for further experiments. Etoposide-treated cells showed polygonal morphology similar to that of primary human hepatocytes (PHHs) (Fig. 1D). Similar to adult PHH organoids, etoposide-treated HLCs lacked strong nucleolar staining (Fig. 1E). At 10 μM, etoposide increased mitochondrial cristae elongation (Fig. 1F), resembling metabolically active PHHs, whereas control HLCs showed mitochondrial vacuolization. The TUNEL and comet assays revealed no significant differences in DNA damage between the treated and control groups (Fig. 1G and H). Flow cytometric analysis of H2AX phosphorylation showed no differences between groups (Fig. 1I). These results confirmed that 10 μM etoposide is non-toxic and does not cause DNA damage in HLCs.

We further evaluated the effect of 10 μM etoposide on HLC senescence by measuring the β-galactosidase activity using flow cytometry and RT-qPCR. No significant differences were observed between the treated and control groups (Fig. 1J and K), indicating that etoposide does not induce senescence. Quiescence is relevant in iPSC-derived hepatocytes, marking terminal differentiation in disease modeling and drug development (17). *CDKN1A* expression increases during both cellular senescence and quiescence, whereas *MKI67* expression is down-regulated

in quiescent hepatocytes. RT-qPCR showed that 10 μM etoposide increased *CDKN1A* expression and decreased *MKI67* expression (Fig. 1L). Overall, 10 μM etoposide did not induce apoptosis, DNA damage, or senescence in HLCs but potentially induced quiescence.

RNA-Seq Reveals Etoposide-Induced Transcriptome Rewiring and Cell Cycle Arrest in HLCs

Low-dose etoposide facilitates osteogenesis in certain cell lines (18) and shifts apoptotic pathways from caspase-dependent to differentiation-linked (19). To further evaluate the effects of etoposide on HLCs, RNA sequencing was performed. Intra-group correlations were higher than inter-group correlations, with control and treated HLCs being similar to PHHs (Fig. 2A). PCA showed that etoposide changed the expression profile of HLCs compared to that of the controls (Fig. 2B), with PC1 accounting for cell source variance (41.25%) and PC2 accounting for etoposide treatment (27.3%). A Venn diagram revealed that 3,301 genes were exclusively expressed in etoposide-treated HLCs (Fig. 2C). Etoposide induced the downregulation of global gene expression (Fig. 2D), with *TOP2A* being the most downregulated. Although etoposide inhibited both TOP2A and TOP2B isoforms, *TOP2B* expression remained unchanged at 10 μM. Among the 1,010 differentially expressed genes, etoposide-induced changes made HLCs resemble PHHs (Fig. 2E). These genes are associated with chromosome segregation, nuclear division, and cell cycle arrest (Fig. 2F). Although etoposide typically causes cell cycle arrest via DNA damage (20), this was not observed in HLCs. Analysis showed that etoposide-treated HLCs resembled PHHs more than control HLCs (Fig. 2G), with the downregulation of cell cycle progression genes. Seventeen genes formed the predicted protein interaction core (Fig. 2H). ChEA analysis identified FOXM1 and E2F4 as the main enriched

transcription factors (Fig. 2I). FOXM1 regulates cell cycle progression (21), suggesting an involvement of FOXM1 in the maturation of HLCs.

Next, to characterize the cell cycle arrest caused by etoposide in HLCs, we found that 10 μM etoposide showed isoform specificity and reduced *TOP2A*, but not *TOP2B*, gene expression (Fig. 2J). Cell cycle arrest was confirmed by reduced *MKI67* and *FOXM1* expression levels, which were similar to those observed in PHHs. Downregulation of *CENPF* and *PLK1* expression (Fig. 2K) was correlated with hepatocyte polyploidization during embryonic liver development (22), indicating that TOP2A inhibition may induce cytokinesis failure and hepatocyte polyploidization. Overall, RNA-seq indicated that treating HLCs with etoposide shifted their transcriptional profile towards PHHs, especially regarding cell cycle regulation gene sets.

TOP2A Inhibition Remodels Chromatin Architecture to Suppress Wnt/JAK-STAT Signaling and Cell Cycle Gene Expression

To assess the effect of TOP2A inhibition on chromatin accessibility, we conducted ATAC-seq on etoposide-treated HLCs and their controls. Etoposide induces global chromatin remodeling and transcriptional silencing (23). In etoposide-treated HLCs, we observed an increase in short-range promoter peak identification (Fig. 3A) but a decrease in overall chromatin accessibility (Fig. 3B). The volcano plot illustrates this reduced chromatin accessibility (Fig. 3C), which accounts for the transcriptional repression observed in the RNA-seq analysis (Fig. 2D). Hierarchical clustering revealed a clear distinction between the treated and control groups, with treated HLCs exhibiting less accessible peaks (Fig. 3D) aligned with gene silencing (Fig. 2E). KEGG analysis indicated alterations in Wnt and JAK-STAT pathways (Fig. 3E), which are crucial for fetal hepatocyte proliferation (10). The PI3K-Akt pathway influences the effects of

Wnt signaling (24). After treatment, chromatin accessibility to PI3K-Akt pathway effectors increased (Fig. 3F). CTCF, which is linked to Wnt signaling (25), emerged as the most differentially enriched motif between the groups (Fig. 3G). Changes in CTCFL expression suggested reduced binding (Fig. 3H). IGV visualization confirmed the decreased accessibility of gene promoters related to hepatocyte proliferation and polyploidization (Fig. 3I).

TOP2B interacts with CTCF and influences gene expression through its topological structure (26). In HLCs, 10 μM etoposide inhibited TOP2A, but not TOP2B, and Hi-C analysis of differentially expressed genes revealed no significant changes in chromatin contacts (Fig. 3J), suggesting that expression changes were independent of genome architecture. TAD and loop analyses demonstrated high similarity across samples, with HLCs and controls exhibiting greater boundary and loop strength concordance (6,537) than PHHs (4,314 in control, 4,521 in treated) (Fig. 3K). The PHHs displayed stronger loop anchor contacts ($p=0.016$) (Supplementary Fig. S2B), and a more distinct compartmentalization beyond 40 Mb (Supplementary Fig. S2D). These findings indicate that etoposide reduced chromatin accessibility and facilitated transcriptional cell cycle arrest via Wnt signaling while preserving the PHH 3D landscape regardless of treatment.

FOXM1 Modulates β-Catenin Signaling and Suppresses Fetal Markers

FOXM1 regulates TOP2A expression and interacts with beta-catenin (27). We administered RCM-1, an inhibitor of FOXM1, to HLCs for five days (Fig. 4A). RCM-1 is known to reduce cell proliferation and induce apoptosis (28). The CellTiter-Glo assay indicated that concentrations exceeding 30 μM diminished the HLC viability (Fig. 4B). At a concentration of 1 μM RCM-1 (chosen for all subsequent assays), immunofluorescence staining demonstrated a reduction in both FOXM1 and phosphorylated Thr600 FOXM1 (pFOXM1) levels (Fig. 4C).

The HLCs treated with etoposide exhibited decreased pFOXM1 levels, suggesting impaired nuclear translocation. In HLCs treated with RCM-1, *TOP2A*, but not *TOP2B* (Fig. 4D). Following treatment with etoposide and RCM-1, the expression of *FOXM1* and *MKI67* decreased. While *ALB* and *HNF4A* levels remained stable, *AFP* expression decreased with FOXM1 inhibition. Both treatments decreased *CTNNB1* expression (Fig. 4E), indicating cell cycle arrest through FOXM1 modulation.

To further investigate the effects of FOXM1 inhibition, phosphoproteomic analysis revealed that etoposide and RCM-1 formed distinct clusters compared with the controls (Fig. 4F). RCM-1 induced a more significant downregulation of proteins than etoposide and controls (Fig. 4G). We identified 90 differentially abundant proteins, most of which were down-regulated (Fig. 4H). The top proteins include fetal hemoglobins (HBG1 and HBG2), UGT2B7, and ASGR1, which are expressed in fetal tissues (29, 30, 31). ChEA analysis highlighted enriched LXR and RXR terms (Fig. 4I) that are crucial for mature hepatocyte lipid metabolism, detoxification, and differentiation (32). The X2K aptamer identified HNF4A/G and FOXA2 as transcription factors, RXRA/B/G and TP53 as intermediate proteins, and GSK3B and ATM as kinases (Fig. 4J). These factors are involved in regulating liver development, proliferation, and differentiation (24, 33, 34), suggesting a role for FOXM1 in the liver development pathways.

Next, we analyzed protein abundance using western blotting to validate qPCR and phosphoproteomic findings. FOXM1 inhibition maintained ALB protein levels while reducing AFP levels (Fig. 4K), consistent with gene expression patterns (Fig. 4E). Although RCM-1 reduced TOP2A expression (Fig. 4D), the TOP2A protein levels remained unchanged. β-catenin abundance decreased after TOP2 inhibition, and was depleted by FOXM1 inhibition (Fig. 4K). Wnt signaling enhances YAP/TAZ activity in fetal hepatocytes, whereas the Hippo pathway suppresses YAP/TAZ activity in adult hepatocytes to maintain differentiation. Thus,

we evaluated TAZ and SMAD1 protein abundance and identified a significant reduction in TAZ upon RCM-1 treatment (Fig. 4K). Overall, FOXM1 modulated the β-catenin pathway and suppressed hepatocyte fetal markers, potentially promoting hepatocyte maturation.

FOXM1 Inhibition Promotes Metabolic Maturation and Polyploidization of HLCs

To assess the long-term effects of TOP2A and FOXM1 inhibition on hepatocyte maturation, HLCs were treated with etoposide and RCM-1 until day 41 of differentiation (D41) (Supplementary Fig. S3A). The lactate dehydrogenase (LDH) release assay revealed no significant cytotoxicity (Supplementary Fig. S3B). In D41 HLCs, *TOP2A*, *FOXM1*, and *MKI67* were significantly downregulated (Supplementary Fig. S3C), indicating cell cycle arrest. *ALB* expression increased with TOP2A inhibition, whereas *AFP* expression decreased under both conditions (Supplementary Fig. S3D). *HNF4A* was also significantly downregulated, suggesting the loss of fetal characteristics and induction of adult hepatic function, as the HNF4A P2 isoform decreases postnatally (35). *E2F1* and *E2F8* polyploidization markers that were decreased in adult hepatocytes (36) were downregulated by FOXM1 inhibition but not by TOP2A (Supplementary Fig. S3E).

To evaluate functional HLC maturation, we investigated mononucleated and binucleated polyploidization (37). In the human liver, 30% of hepatocytes are polyploid because of cytokinesis failure during early postnatal life (29). Flow cytometry with PI staining revealed that etoposide increased mononucleated polyploidy by 27.6%, whereas RCM-1 led to a 7.4% increase (Fig. 5A). To assess the trade-off between hepatocyte proliferation and metabolic maturation, we assessed HLC metabolic maturation upon inducing cell cycle arrest (38). We observed enhanced CYP1A2 and CYP2B6 activities with FOXM1 inhibition (~2.5×), whereas TOP2 inhibition only increased CYP1A2 (Fig. 5B). The upregulation of CYP1A2 with RCM-

1 may be linked to AHR signaling (39, 40), whereas CYP2B6 upregulation might involve PXR/RXR signaling (41), consistent with our phosphoproteomic findings (Fig. 4I). These pathways are essential for xenobiotic metabolism during terminal differentiation (42). RCM-1 treatment resulted in increased cholesterol secretion (~1.9×) and decreased triglyceride secretion (~4.2×) in HLCs (Fig. 5C), indicating enhanced APOB production and effective lipid homeostasis (43, 44). In assessing hepatocyte damage, secreted ALT levels were higher in the controls, whereas AST levels showed no difference (Fig. 5D). Both ALB and AFP levels decreased during maintenance, with a significant reduction in AFP levels in the treated hepatocytes (Fig. 5E). Western blotting indicated unchanged levels of ALB, CTNNB1, and ERK1/2, but a notable reduction in AFP in the RCM-1-treated groups (~5.6×) (Fig. 5F).

In summary, we found that long-term TOP2 and FOXM1 inhibition resulted in no cytotoxicity and induced mononucleated hepatocyte polyploidization. In addition, only FOXM1 inhibition was associated with HLC metabolic maturation and fetal protein downregulation, potentially indicating the consistent in vitro terminal differentiation of hiPSC-derived hepatocytes.

DISCUSSION

We explored the roles of TOP2A and FOXM1 in the terminal differentiation of HLCs, a critical aspect of liver modeling that current protocols have yet to fully achieve. Inhibition of FOXM1 promoted the terminal differentiation of HLCs by inducing cell cycle arrest, polyploidization, and metabolic maturation, while reducing fetal markers. The transition from the fetal to adult stage is governed by the Wnt/β-Catenin Pathway (45, 46). FOXM1 inhibition leads to a decrease in Wnt target expression (47) and β-catenin expression, highlighting its significance in hepatocyte maturation. Prolonged FOXM1 inhibition enhanced CYP1A2 and CYP2B6 activities and improved lipid metabolism. miR-122 is essential for hepatocyte polyploidization

and targets FOXM1 (46), indicating that FOXM1 downregulation may contribute to miR-122-dependent terminal hepatocyte maturation. Extended FOXM1 inhibition results in a doubling of mononucleated hepatocyte ploidy, which is linked to the maturation of HLC lipid metabolism. FOXM1 upregulates TOP2A expression by binding to its promoter (48). TOP2A facilitates cell cycle progression during liver development (49) and its downregulation is associated with hepatocyte maturation (50). Long-term inhibition of TOP2A increases HLC polyploidization to levels observed in adult livers and enhances ALB expression, whereas short-term inhibition reduces chromatin accessibility and silences cell cycle genes. Overall, the mutual regulation of TOP2A and FOXM1 may be vital for the late-stage maturation of HLCs.

Although we studied FOXM1 and TOP2A in the terminal differentiation of HLCs, postnatal development creates hepatocyte subpopulations via liver zonation (46). FOXM1 and TOP2A modulation in vitro may produce interzonal-like hepatocytes owing to the lack of metabolic compartmentalization in our system (51). Thus, pericentral, periportal, and interzonal hepatocyte differentiation require further study. To improve hepatocyte maturation, we proposed targeting FOXM1 and TOP2A using 3D hepatocyte differentiation protocols for a more physiological model, as these enable three-dimensional cell interactions and native extracellular matrix reproduction (52). Our approach was limited to hepatocytes, excluding interactions between parenchymal and non-parenchymal liver cells. However, iPSCs can produce cholangiocytes, hepatic stellate cells, and Kupffer cells, which are essential for modeling liver disease, and their interactions documented in liver organoid models must be accounted for in the development and disease modeling (53). Finally, FOXM1 knockout murine models showed abnormal hepatocyte polyploidization, suggesting that FOXM1 modulation requires fine-tuning during late development (36). Thus, further in vivo studies are needed to validate our findings on FOXM1 and TOP2A modulation of liver development.

Despite our understanding of cell cycle regulation during hepatocyte terminal maturation, there is a lack of clarity regarding how these mechanisms function during embryonic liver development, regeneration, and cancer. Therefore, we hypothesized that FOXM1 was a key candidate for hepatocyte cell cycle regulation. FOXM1 is crucial for hepatocyte cell cycle entry post hepatectomy, promoting essential proteins such as cyclin A2 and B1 for mitotic progression (54). FOXM1 promotes hepatocyte proliferation and liver mass restoration through its interaction with Wnt/β-catenin signaling (55). Although FOXM1 facilitates regeneration, its overexpression can promote liver cancer (56), which is correlated with malignancy and poor prognosis (57). FOXM1 inhibition using small molecules reduces hepatocellular carcinoma growth (58), and experimental models have shown decreased tumorigenic capabilities (59). Thus, investigation of FOXM1 modulation may be critical for understanding liver regeneration and carcinogenesis.

In summary, our results indicated that FOXM1 inhibition in HLCs is associated with enhanced hepatocyte terminal differentiation, characterized by cell cycle arrest, polyploidization, and metabolic maturation.

MATERIALS AND METHODS

Treatment with small molecules

For topoisomerase II inhibition, 10 mM etoposide (Sigma-Aldrich, Saint Louis, Missouri, USA) was dissolved in dimethyl sulfoxide (DMSO). For FOXM1 inhibition, 2 mM RCM-1 (Sigma-Aldrich) was dissolved in dimethyl sulfoxide (DMSO) and Etoposide or RCM-1 was diluted in DMSO at 100x a final intended concentration. Next, 100x etoposide or RCM-1 was directly added to the hepatocyte maturation medium and diluted 1:100. Etoposide was

predominantly used at a final concentration of 10 μM, whereas RCM-1 was used at a final concentration of 1 μM. The control groups were treated with 1% DMSO in hepatocyte maturation medium. The medium was changed every 48h, and the treatments were initiated on differentiation day 20.

RNA-extraction, RT-qPCR, and RNA-sequencing analysis

RNA was extracted using a PureLink RNA Mini Kit (Thermo Fisher Scientific). Reverse transcription was performed using the Superscript IV Synthesis Kit (Thermo Fisher Scientific). RT-qPCR was performed using Power SYBR Green PCR Master Mix (Thermo Fisher) on a QuantStudio 5 System. The samples were amplified using primers designed using Primer-BLAST or retrieved from PrimerBank (Supplementary Table 1). Expression analysis was performed using the ΔΔCt method and normalized to the RPLP0 or GUSB controls. Human Plateable Hepatocytes were used as the PHH controls and were harvested for 24h. RNA sequencing was performed using the Novogene software. RNA quality was assessed using Bioanalyzer 2100 (Agilent). Library preparation was performed using the TruSeq Stranded mRNA Kit, and sequencing was performed using NovaSeq 6000 (Illumina). The reads were aligned to the human genome hg38 using Hisat2. Differential gene expression analysis was performed using the DESeq2 package in R. The thresholds for differential expression were adjusted P-value ≤ 0.05, and $|\log2(\text{fold change})| \geq 1$. ClusterProfiler was used to test the enrichment of differentially expressed genes. Data visualization was performed using the clusterProfiler and pheatmap packages and the MaGIC Volcano Plot Tool. PPI analysis was performed using the STRING database and term enrichment was performed using the Enrichr web tool.

ATAC-sequencing analysis

ATAC sequencing was conducted through Novogene. Nuclei were incubated with a Tn5 transposase mix at 37°C for 30 minutes. Libraries underwent PCR amplification, were purified using AMPure beads, and evaluated with Qubit. Sequencing was performed on the Illumina Hiseq Platform, producing 150 bp paired-end reads. Reads were trimmed with Skewer, aligned using BWA, and filtered for quality (MAPQ 13) and proper pairing (>18 nt). Peak calling was executed with macs2 using the command 'macs2 callpeak --nomodel --keepdup all-call summits (v2.1.2). Term enrichment was analyzed with Enrichr, and motifs were identified using HOMER. The ATAC-seq library preparation adhered to the ATAC 2.0 protocol. Cells were fixed with paraformaldehyde, quenched with glycine, and stored at −80°C. Following lysis, cells were digested with DpnII, labeled with biotin-14-dCTP, and ligated. Libraries were prepared using the KAPA HyperPlus Kit with biotin enrichment. Data processing was carried out with Juicer and Cooltools. Normalized maps were analyzed using FANC, and compartmentalization was assessed with cooltools saddle functions. A/B compartments were assigned through eigenvector decomposition.

Proteomic analysis

For proteomic analysis, samples were lysed using buffer containing 50 mM HEPES (pH 8), 1% SDS, 1% sodium deoxycholate, 5 mM EDTA, and 50 mM NaCl, with Halt Protease and Phosphatase Inhibitor Cocktail. Proteins were quantified using the Pierce BCA Protein Assay Kit, and 250 µg in 100 µL was digested using a modified semi-automated SP3 protocol. Phosphopeptides were enriched using titanium dioxide beads (Titansphere, Gl Sciences, Japan), according to the manufacturer's instructions. LC-MS/MS analyses were performed using a nano LC UltiMate 3000 system connected to an Exploris 240 hybrid quadrupole-

orbitrap tandem mass spectrometer (Thermo Fisher Scientific, Bremen, Germany) equipped with an EASY-spray source operating in positive ion mode. Spectral data were searched against an in silico human spectral library (Uniprot Swissprot database downloaded on August 06, 2024, which contained 20,447 entries) using DIA-NN 1.9.1. FragPipe-Analyst was used for visualization, Enrichr for term enrichment, and X2K web tool for regulatory networks.

Flow cytometry analysis

For flow cytometry analysis, the cells were dissociated using TrypLE Express Enzyme (Thermo Fisher Scientific). The cells were fixed and permeabilized using the Fix & Perm Cell Fixation and Permeabilization Kit (Thermo Fisher Scientific), according to the manufacturer's instructions. The samples were blocked with 5% BSA in PBS (1x) for 1 h and then incubated with primary antibodies (listed in Supplementary Table 3) at 4ºC for 1h. After washing with PBS (1x), the samples were incubated with Alexa Fluor-conjugated secondary antibodies (Supplementary Table 3) at 4°C for 1 h. The samples were analyzed using a FACS Aria III flow cytometer (BD Biosciences) with 20,000 events per group. For ploidy analysis, samples were dissociated with TrypLE Express (Thermo Fisher), fixed with 70% ethanol at -20ºC for 2h, and DNA was stained using FxCycle PI/RNase Staining Solution (Thermo Fisher) with 100 U/µL RNase I for 30 min at 37°C, acquiring 500,000 cells per group. For DNA fragmentation and damage assays, we used the Click-iT TUNEL Alexa Fluor 488 kit and an anti-phospho-H2AX antibody (Supplementary Table 3). The CellEvent Senescence Green Flow Cytometry Assay Kit (Thermo Fisher Scientific) was used for senescence evaluation. Data were analyzed using the FlowJo V10 software.

Toxicity assays

For the cytotoxicity assays, HLCs were differentiated into 96-well plates. To assess cell viability, intracellular ATP levels were measured using the CellTiter-Glo Luminescent Cell Viability Assay Kit (Promega, G7571), according to the manufacturer's instructions. To assess toxicity, 200 μL of the supernatant was collected and lactate dehydrogenase (LDH) was measured using the CyQUANT LDH Cytotoxicity Assay (Thermo Fisher, C20301), according to the manufacturer's instructions. Both assays were normalized using a blank negative control (hepatocyte maturation medium) and death-positive control (5% Triton-X100 treatment for 15 min).

Quantification and statistical analysis

Statistical analyses were performed using GraphPad Prism 8 with an unpaired two-tailed Student's t-test, one-way analysis of variance (ANOVA), and post-hoc Tukey's test. Statistical significance was set at $P < 0.05$. n represents number of biological replicates and independent experiments. G*Power software was used to determine the minimum sample size for data collection to achieve $\alpha = 0.05$ and power =p0.8.

REFERENCES

1. Kehtari M, Zeynali B, Soleimani M, Kabiri M, Seyedjafari E. Fabrication of a co-culture micro-bioreactor device for efficient hepatic differentiation of human induced pluripotent stem cells (hiPSCs). Artif Cells Nanomed Biotechnol. 2018;46:161–170.

2. Du C, Feng Y, Qiu D, Xu Y, Pang M, Cai N, et al. Highly efficient and expedited hepatic differentiation from human pluripotent stem cells by pure small-molecule cocktails. Stem Cell Res Ther. 2018;9.

3. Akbari S, Sevinç GG, Ersoy N, Basak O, Kaplan K, Sevinç K, et al. Robust, Long-Term Culture of Endoderm-Derived Hepatic Organoids for Disease Modeling. Stem Cell Reports. 2019;13:627–641.

4. Graffmann N, Scherer B, Adjaye J. In vitro differentiation of pluripotent stem cells into hepatocyte like cells – Basic principles and current progress. Stem Cell Res. 2022;61.

5. Telles-Silva KA, Pacheco L, Komatsu S, Chianca F, Caires-Júnior LC, Araujo BHS, et al. Applied Hepatic Bioengineering: Modeling the Human Liver Using Organoid and Liver-on-a-Chip Technologies. Front Bioeng Biotechnol. 2022;10.

6. Pommier Y, Nussenzweig A, Takeda S, Austin C. Human topoisomerases and their roles in genome stability and organization. Nat Rev Mol Cell Biol. 2022;23.

7(11). Wang H, Liu J, Zhu P, Shi L, Liu Y, Yang X, et al. Single-nucleus transcriptome reveals cell dynamic response of liver during the late chick embryonic development. Poult Sci. 2024;103.

8. Uusküla-Reimand L, Wilson MD. Untangling the roles of TOP2A and TOP2B in transcription and cancer. Sci Adv [Internet]. 2022 [cited 2025 Apr 30];8:eadd4920. Available from: https://pmc.ncbi.nlm.nih.gov/articles/PMC9629710/

9. Yu G, Zhang S, Romo A, Biswas S, Li B, Li J. Liver regeneration by a population of midzone-located mesenchymal-hepatocyte hybrid cells. 2024 [cited 2025 Apr 30];Available from: https://elifesciences.org/reviewed-preprints/92531

10. Sun X, Liu Y, Zhou S, Wang L, Wei J, Hua R, et al. Circular dorsal ruffles disturb the growth factor-induced PI3K-AKT pathway in hepatocellular carcinoma Hep3B cells. Cell Communication and Signaling. 2022;20.

11. Chand V, Pandey A, Kopanja D, Guzman G, Raychaudhuri P. Opposing Roles of the Fork-head box genes FoxM1 and FoxA2 in Hepatocellular Carcinoma. 2018 [cited 2025 Apr 30];Available from: http://biorxiv.org/lookup/doi/10.1101/383604

12. Hsu CC, Yao X, Chen SY, Tsuo TC, Wang IC. The conformation of FOXM1 homodimers in vivo is crucial for regulating transcriptional activities. Nucleic Acids Res. 2024;52:13625–13643.

13. Krupczak-Hollis K, Wang X, Kalinichenko V V., Gusarova GA, Wang IC, Dennewitz MB, et al. The mouse Forkhead Box m1 transcription factor is essential for hepatoblast mitosis and development of intrahepatic bile ducts and vessels during liver morphogenesis. Dev Biol. 2004;276:74–88.

14. Gupta R, Schrooders Y, Hauser D, van Herwijnen M, Albrecht W, ter Braak B, et al. Comparing in vitro human liver models to in vivo human liver using RNA-Seq. Arch Toxicol. 2021;95:573–589.

15. Gordillo M, Evans T, Gouon-Evans V. Orchestrating liver development. Development [Internet]. 2015 [cited 2025 Apr 30];142:2094. Available from: https://pmc.ncbi.nlm.nih.gov/articles/PMC4483763/

16. Baranski OA, Kalinichenko V V., Adami GR. Increased FOXM1 expression can stimulate DNA repair in normal hepatocytes in vivo but also increases nuclear foci associated with senescence. Cell Prolif. 2015;48:105–115.

17. Payea MJ, Dar SA, Anerillas C, Martindale JL, Belair C, Munk R, et al. Senescence suppresses the integrated stress response and activates a stress-remodeled secretory phenotype. Mol Cell. 2024;84:4454-4469.e7.

18. Yang M, Tian X, Fan Z, Yu W, Li Z, Zhou J, et al. Targeting RAD51 enhances chemosensitivity of adult T-cell leukemia-lymphoma cells by reducing DNA double-strand break repair. Oncol Rep. 2019;42:2426–2434.

19. Melo-Hanchuk TD, Slepicka PF, Pelegrini AL, Menck CFM, Kobarg J. NEK5 interacts with topoisomerase IIβ and is involved in the DNA damage response induced by etoposide. J Cell Biochem. 2019;120:16853–16866.

20. Wilkinson PD, Delgado ER, Alencastro F, Leek MP, Roy N, Weirich MP, et al. The Polyploid State Restricts Hepatocyte Proliferation and Liver Regeneration in Mice. Hepatology. 2019;69:1242–1258.

21. Matsumoto T, Wakefield L, Tarlow BD, Grompe M. In Vivo Lineage Tracing of Polyploid Hepatocytes Reveals Extensive Proliferation during Liver Regeneration. Cell Stem Cell. 2020;26:34-47.e3.

22. Xiong X, Kuang H, Ansari S, Liu T, Gong J, Wang S, et al. Landscape of Intercellular Crosstalk in Healthy and NASH Liver Revealed by Single-Cell Secretome Gene Analysis. Mol Cell. 2019;75:644-660.e5.

23. Ji Z, Zhang L, Peng V, Ren X, McHale CM, Smith MT. A comparison of the cytogenetic alterations and global DNA hypomethylation induced by the benzene metabolite, hydroquinone, with those induced by melphalan and etoposide. Leukemia 2010 24:5 [Internet]. 2010 [cited 2025 Apr 30];24:986–991. Available from: https://www.nature.com/articles/leu201043

24. Wang C, He Q, Yin Y, Wu Y, Li X. Clonorchis sinensis Granulin Promotes Malignant Transformation of Hepatocyte Through EGFR-Mediated RAS/MAPK/ERK and PI3K/Akt Signaling Pathways. Front Cell Infect Microbiol. 2021;11.

25. Wu S-X, Chen W-N, Jing Z-T, Liu W, Lin X-J, Lin X. Hepatitis B Spliced Protein (HBSP) Suppresses Fas-Mediated Hepatocyte Apoptosis via Activation of PI3K/Akt Signaling. J Virol. 2018;92.

26. Pommier Y, Nussenzweig A, Takeda S, Austin C. Human topoisomerases and their roles in genome stability and organization. Nature Reviews Molecular Cell Biology 2022 23:6 [Internet]. 2022 [cited 2025 Apr 30];23:407–427. Available from: https://www.nature.com/articles/s41580-022-00452-3

27. Chen Y, Li Y, Xue J, Gong A, Yu G, Zhou A, et al. Wnt-induced deubiquitination FoxM1 ensures nucleus β-catenin transactivation. EMBO J. 2016;35:668–684.

28. Shukla S, Milewski D, Pradhan A, Rama N, Rice K, Le T, et al. The FOXM1 inhibitor RCM-1 decreases carcinogenesis and nuclear b-catenin. Mol Cancer Ther. 2019;18:1217–1229.

29. Huse SM, Gruppuso PA, Boekelheide K, Sanders JA. Patterns of gene expression and DNA methylation in human fetal and adult liver. BMC Genomics. 2015;16.

30. Cappiello M, Giuliani L, Rane A, Pacifici GM. Uridine 5′-diphosphoglucuronic acid (UDPGLcUA) in the human fetal liver, kidney and placenta. Eur J Drug Metab Pharmacokinet. 2000;25:161–163.

31. Elagooz R, Dhara AR, Gott RM, Adams SE, White RA, Ghosh A, et al. PUM1 mediates the posttranscriptional regulation of human fetal hemoglobin. Blood Adv. 2022;6:6016–6022.

32. Benítez-Santana T, Hugo SE, Schlegel A. Role of intestinal LXRa in regulating post-prandial lipid excursion and diet-induced hypercholesterolemia and hepatic lipid accumulation. Front Physiol. 2017;8.

33. Thakur A, Wong JCH, Wang EY, Lotto J, Kim D, Cheng JC, et al. Hepatocyte Nuclear Factor 4-Alpha Is Essential for the Active Epigenetic State at Enhancers in Mouse Liver. Hepatology [Internet]. 2019 [cited 2025 Apr 30];70:1360–1376. Available from: https://journals.lww.com/hep/fulltext/2019/10000/hepatocyte_nuclear_factor_4_alpha_is_essential_for.24.aspx

34. Timmerman DM, Remmers TL, Hillenius S, Looijenga LHJ. Mechanisms of TP53 Pathway Inactivation in Embryonic and Somatic Cells—Relevance for Understanding (Germ Cell) Tumorigenesis. International Journal of Molecular Sciences 2021, Vol. 22, Page 5377 [Internet]. 2021 [cited 2025 Apr 30];22:5377. Available from: https://www.mdpi.com/1422-0067/22/10/5377/htm

35. Kotulkar M, Robarts DR, Apte U. HNF4α in Hepatocyte Health and Disease. Semin Liver Dis. 2023;43:234–244.

36. Sladky VC, Knapp K, Szabo TG, Braun VZ, Bongiovanni L, van den Bos H, et al. PIDDosome-induced p53-dependent ploidy restriction facilitates hepatocarcinogenesis. EMBO Rep. 2020;21.

37. Windmueller R, Leach JP, Babu A, Zhou S, Morley MP, Wakabayashi A, et al. Direct Comparison of Mononucleated and Binucleated Cardiomyocytes Reveals Molecular Mechanisms Underlying Distinct Proliferative Competencies. Cell Rep. 2020;30:3105-3116.e4.

38. Llorens-Giralt P, Ruiz-Romero M, Nurtdinov R, Herranz-Itúrbide M, et al. Sequential activation of transcription factors promotes liver regeneration through specific and developmental enhancers. Cell Genom. 2025; 20:100887.

39. Turpeinen M, Raunio H, Pelkonen O. The Functional Role of CYP2B6 in Human Drug Metabolism: Substrates and Inhibitors In Vitro, In Vivo and In Silico. Curr Drug Metab [Internet]. 2006 [cited 2025 Apr 30];7:705–714. Available from: https://www.eurekaselect.com/article/2842

40. Smith BW, Stanford EA, Sherr DH, Murphy GJ. Genome Editing of the CYP1A1 Locus in iPSCs as a Platform to Map AHR Expression throughout Human Development. Stem Cells Int. 2016;2016.

41. Kondo Y, Iwao T, Nakamura K, Sasaki T, Takahashi S, Kamada N, et al. An efficient method for differentiation of human induced pluripotent stem cells into hepatocyte-like cells retaining drug metabolizing activity. Drug Metab Pharmacokinet. 2014;29:237–243.

42. Rakateli L, Huchzermeier R, van der Vorst EPC. AhR, PXR and CAR: From Xenobiotic Receptors to Metabolic Sensors. Cells 2023, Vol. 12, Page 2752 [Internet]. 2023 [cited 2025 Apr 30];12:2752. Available from: https://www.mdpi.com/2073-4409/12/23/2752/htm

43. Krueger WH, Tanasijevic B, Barber V, Flamier A, Gu X, Manautou J, et al. Cholesterol-Secreting and Statin-Responsive Hepatocytes from Human ES and iPS Cells to Model Hepatic Involvement in Cardiovascular Health. PLoS One. 2013;8.

44. Surugihalli C, Porter TE, Chan A, Farley LS, Maguire M, Zhang C, et al. Hepatic Mitochondrial Oxidative Metabolism and Lipogenesis Synergistically Adapt to Mediate Healthy Embryonic-to-Neonatal Transition in Chicken. Sci Rep. 2019;9.

45. Moreno-Marín N, Merino JM, Alvarez-Barrientos A, Patel DP, Takahashi S, González-Sancho JM, et al. Aryl Hydrocarbon Receptor Promotes Liver Polyploidization and Inhibits PI3K, ERK, and Wnt/β-Catenin Signaling. Food Science and Human Wellness [Internet]. 2018 [cited 2025 Apr 30];4:44–63. Available from: https://pubmed.ncbi.nlm.nih.gov/30240752/

46. Reza H Al, Santangelo C, Iwasawa K, Reza A Al, Sekiya S, Glaser K, et al. Multi-zonal liver organoids from human pluripotent stem cells. Nature 2025 [Internet]. 2025 [cited 2025 Apr 30];1–10. Available from: https://www.nature.com/articles/s41586-025-08850-1

47. Kim JY, Choi H, Kim HJ, Jee Y, Noh M, Lee MO. Polyploidization of Hepatocytes: Insights into the Pathogenesis of Liver Diseases. Biomol Ther (Seoul). 2022;30:391–398.

48. Ahmed F. Integrated Network Analysis Reveals FOXM1 and MYBL2 as Key Regulators of Cell Proliferation in Non-small Cell Lung Cancer. Front Oncol. 2019;9.

49. Enomoto H, Yoshida K, Kishima Y, Kinoshita T, Yamamoto M, Everett AD, et al. Hepatoma-derived growth factor is highly expressed in developing liver and promotes fetal hepatocyte proliferation. Hepatology [Internet]. 2002 [cited 2025 Apr 30];36:1519–1527. Available from: https://journals.lww.com/hep/fulltext/2002/12000/hepatoma_derived_growth_factor_is_highly_expressed.28.aspx.

50. Thakurela S, Garding A, Jung J, Schübeler D, Burger L, Tiwari VK. Gene regulation and priming by topoisomerase IIα in embryonic stem cells. Nat Commun [Internet]. 2013 [cited 2025 Apr 30];4:1–13. Available from: https://www.nature.com/articles/ncomms3478.

51. Martini T, Naef F, Tchorz JS. Spatiotemporal Metabolic Liver Zonation and Consequences on Pathophysiology. Annual Review of Pathology: Mechanisms of Disease [Internet]. 2023 [cited 2025 Apr 30];18:439–466. Available from:

https://www.annualreviews.org/content/journals/10.1146/annurev-pathmechdis-031521-024831;jsessionid=uJQ_ojQHgWNaZZG_BB_E2JW6pVrw0WMPPpQEUaQm.annurevlive-10-241-10-100

52. Maepa SW, Ndlovu H. Advances in generating liver cells from pluripotent stem cells as a tool for modeling liver diseases. Stem Cells [Internet]. 2020 [cited 2025 Apr 30];38:606–612. Available from: https://dx.doi.org/10.1002/stem.3154

53. Olgasi C, Cucci A, Follenzi A. iPSC-Derived Liver Organoids: A Journey from Drug Screening, to Disease Modeling, Arriving to Regenerative Medicine. International Journal of Molecular Sciences 2020, Vol. 21, Page 6215 [Internet]. 2020 [cited 2025 Apr 30];21:6215. Available from: https://www.mdpi.com/1422-0067/21/17/6215/htm

54. Sato Y, Katoh Y, Matsumoto M, Sato M, Ebina M, Itoh-Nakadai A, et al. Regulatory signatures of liver regeneration distilled by integrative analysis of mRNA, histone methylation, and proteomics. Journal of Biological Chemistry. 2017;292:8019–8037.

55. Chen Y, Yang Y, Wang N, Liu R, Wu Q, Pei H, et al. β-Sitosterol suppresses hepatocellular carcinoma growth and metastasis via FOXM1-regulated Wnt/β-catenin pathway. J Cell Mol Med. 2024;28.

56. Sheng Y, Yu C, Liu Y, Hu C, Ma R, Lu X, et al. FOXM1 regulates leukemia stem cell quiescence and survival in MLL-rearranged AML. Nat Commun. 2020;11.

57. Song BN, Chu IS. A gene expression signature of FOXM1 predicts the prognosis of hepatocellular carcinoma. Exp Mol Med. 2018;50.

58. Radhakrishnan SK, Bhat UG, Hughes DE, Wang IC, Costa RH, Gartel AL. Identification of a chemical inhibitor of the oncogenic transcription factor forkhead box M1. Cancer Res. 2006;66:9731–9735.

59. Wang I-C, Chen Y-J, Hughes D, Petrovic V, Major ML, Park HJ, et al. Forkhead Box M1 Regulates the Transcriptional Network of Genes Essential for Mitotic Progression and Genes Encoding the SCF (Skp2-Cks1) Ubiquitin Ligase. Mol Cell Biol. 2005;25:10875–10894.

STATEMENTS

Conflict of Interest

The authors declare that they have no competing interests.

Author Contribution

K.A.T-S designed and performed the research, analyzed the data, performed bioinformatics analyses, and wrote the paper. L.P., S.K., F.C., G.C., G.C.M., M.G., D.P., V.M.C., and E.G.C. assisted in RT-qPCR, staining, comet, ATAC-seq, phosphoproteomic, and transmission electron microscopy experiments and revised the manuscript. E.G., M.A., and V.S.F. designed the study and revised the manuscript. M.Z. designed the study and prepared the manuscript.

Ethics

All experiments using human iPSCs were approved by the Ethics Committees of the Biosciences Institute of the University of São Paulo (USP) (Protocol 1.294.118).

Funding

The authors (s) declare that they received financial support for the research, authorship, and/or publication of this article. The authors sincerely acknowledge the support of the São Paulo Research Foundation (FAPESP/CEPID and CCD) (13/08028-1 and 21/11872-5, respectively). K.A.T-S is an FAPESP grant (19/19380–4 and 22/08157–5). L.P., S.K., G.C., and G.C.M are FAPESP grantees (23/10642-1, 23/18178-2, 24/10799-0, and 22/02311-2 respectively). F.C. is a CAPES grantee (88882.461730/2019-01). Hi-C library preparation and sequencing were supported by grants from the State Program of the Sirius Federal Territory Scientific and Technological Development of the Sirius Federal Territory (Agreement nº 26-03, 27/09/2024). We acknowledge the Center for Collective Usage of Computational Facilities of the Institute of Cytology and Genetics (supported by the budget project FWNR-2022-0019), the Fleury Group for proteomics analysis, and the HPC Cluster of the Novosibirsk State University (supported by the Ministry of Science and Higher Education of the Russian Federation, grant no. FSUS-2024-0018) to provide access to computational resources.

Data availability

The RNA-seq, ATAC–seq, and Hi-C data reported in this study have been deposited in the NCBI Gene Expression Omnibus (GEO) with accession numbers GSE298619, GSE298820, and GSE298819, respectively. The proteomic data reported in this study have been deposited

in the ProteomeXchange Consortium via the PRIDE partner repository under accession number PXD064121.

FIGURE LEGENDS

Fig. 1: Low-dose etoposide preserves the viability and DNA integrity of HLCs. A) Schematic of etoposide treatment of HLCs (Created using BioRender.com). **B**) Cell viability assay of HLCs and HepG2s negative control) with different concentrations of etoposide to determine toxic doses (*n* = 2 biological replicates and 3 independent experiments for HLCs, *n* = 3 independent experiments for HepG2). **C**) Cell viability assay of HLCs with different concentrations of etoposide and teniposide to compare toxic doses. **D**) Brightfield images of HLCs treated with 10 μM etoposide (scale bar = 400 μm). **E**) Transmission electron micrograph of etoposide-treated HLCs (scale bar = 5 μm). N = nucleus; Nu = nucleoli; Mit = mitochondria. **F**) Transmission electron micrograph of etoposide-treated HLCs's mitochondria (scale bar = 1 μm). Mit = mitochondria. **G**) TUNEL assay of etoposide-treated HLCs. **H**) COMET assay of etoposide-treated HLCs. **I**) Flow cytometry of pH2AX staining of etoposide-treated HLCs. **J**) Flow cytometry of hydrolyzed β-galactosidase staining of etoposide-treated HLCs. **K**) RT-qPCR of *GLB1* of etoposide-treated HLCs. **L**) RT-qPCR of *CDKN1A* and *MKI67* of etoposide-treated HLCs. In every experiment, *n* = 2 biological replicates and 3 independent experiments. In B, C, H, K, and L, data is mean ± SD. In B and C, paired t-test ($p<0.05$). In H, K, and L, t-test ($p<0.001$).

Fig. 2: RNA-seq analysis of etoposide-treated HLCs. A) Inter-sample correlation matrix heatmap (R^2 = square of Pearson correlation coefficient) of control HLCs, etoposide-treated

HLCs, and primary human hepatocytes (PHHs). **B**) Principal component analysis (PCA) on fragments per kilobase per million mapped fragments (FKPM). **C**) Venn diagram on all identified genes. **D**) Volcano plot of differentially expressed genes between etoposide-treated and control HLCs (|log2(FoldChange)| >= 1 & padj <= 0.05). **E**) Heatmap of the top 100 z-scored differentially expressed genes between etoposide-treated and control HLCs. **F**) Gene ontology (GO) scatter plot for biological processes of the top 100 z-scored differentially expressed genes between etoposide-treated and control HLCs. The size of the circle indicates the percentage of genes in each annotation category. **G**) Heatmap of the top 25 z-scored differentially expressed genes between etoposide-treated and control HLCs. **H**) STRING interactome of the top 25 differentially expressed genes between etoposide-treated and control HLCs. The colours represent k-means clustering. **I**) ChIP-X enrichment analysis (ChEA) of the top 25 differentially expressed genes between etoposide-treated and control HLCs. **J-K**) RT-qPCR of *TOP2A* and *TOP2B* (**J**); or *MKI67*, *FOXM1*, *CENPF*, and *PLK1* (**K**) of etoposide-treated HLCs. In every experiment, $n = 2$ biological replicates. In E and G, the colour represents the average expression level for the indicated gene. In J and K, data is mean ± SD, analyzed by one-way ANOVA with multiple comparisons and Tukey's correction ($p<0.001$); $n = 2$ biological replicates and 3 independent experiments.

Fig. 3: ATAC-seq and Hi-C analysis of etoposide-treated HLCs. **A**) Peak distribution in functional gene regions of control and etoposide-treated HLCs. **B**) Distribution of the reads mapped to the TSS. The colour indicates the average density of reads. **C**) Comparison of global chromatin accessibility. Treatment, etoposide-treated HLCs; Control, control HLCs. **D**) Heatmap of z-scored peak fold enrichment between etoposide-treated and control HLCs. The colour represents the average normalized enrichment per chromatin domain. **E**) KEGG analysis

of the top 100 enriched peak chromatin domains between etoposide-treated and control HLCs. **F**) Transcription factor protein-protein interaction (PPI) analysis of the top 100 enriched peak chromatin domains between etoposide-treated and control HLCs. **G**) Enrichment of motif and known transcription factor motif. The size of the circle indicates the average degree of enrichment of the motif's motif and the corresponding transcription factor's motif. **H**) Motif analysis of the conserved sequence of the peak enrichment position. The motifs are averaged by control or etoposide-treated HLCs and ranked by p-value. **I**) Chromatin accessibility analysis of *TOP2A*, *FOXM1*, *AURKA*, *CCNB1*, *E2F1*, and *PLK1* genes. The peaks represent the average pileup signal for control (blue) or etoposide-treated (green) HLCs. **J**) Chromatin architecture analysis. Hi-C contact maps (observed/expected) at 50 kb resolution for primary human hepatocytes (PHH), control (74C, 87C), and etoposide-treated (74T, 87T) HLCs. Left, *CTCF* genomic region; Right, *NTS* genomic region. **K**) Topologically associating domains (TADs) and insulation scores. Upper left, venn diagram of shared and condition-specific TAD boundaries identified at 25 kb resolution. Upper right and bottom, pairwise comparisons of insulation scores at TAD boundaries between samples. Each point represents an individual TAD boundary; Red dots, outliers with insulation score differences greater than three standard deviations; Blue lines, linear regression trend lines and Pearson correlation coefficient. In every experiment, n = 2 biological replicates. Blue, control HLCs; Green, etoposide-treated HLCs. In E and F, the color and length of the bars indicate the combined ranked p-value and odds ratio.

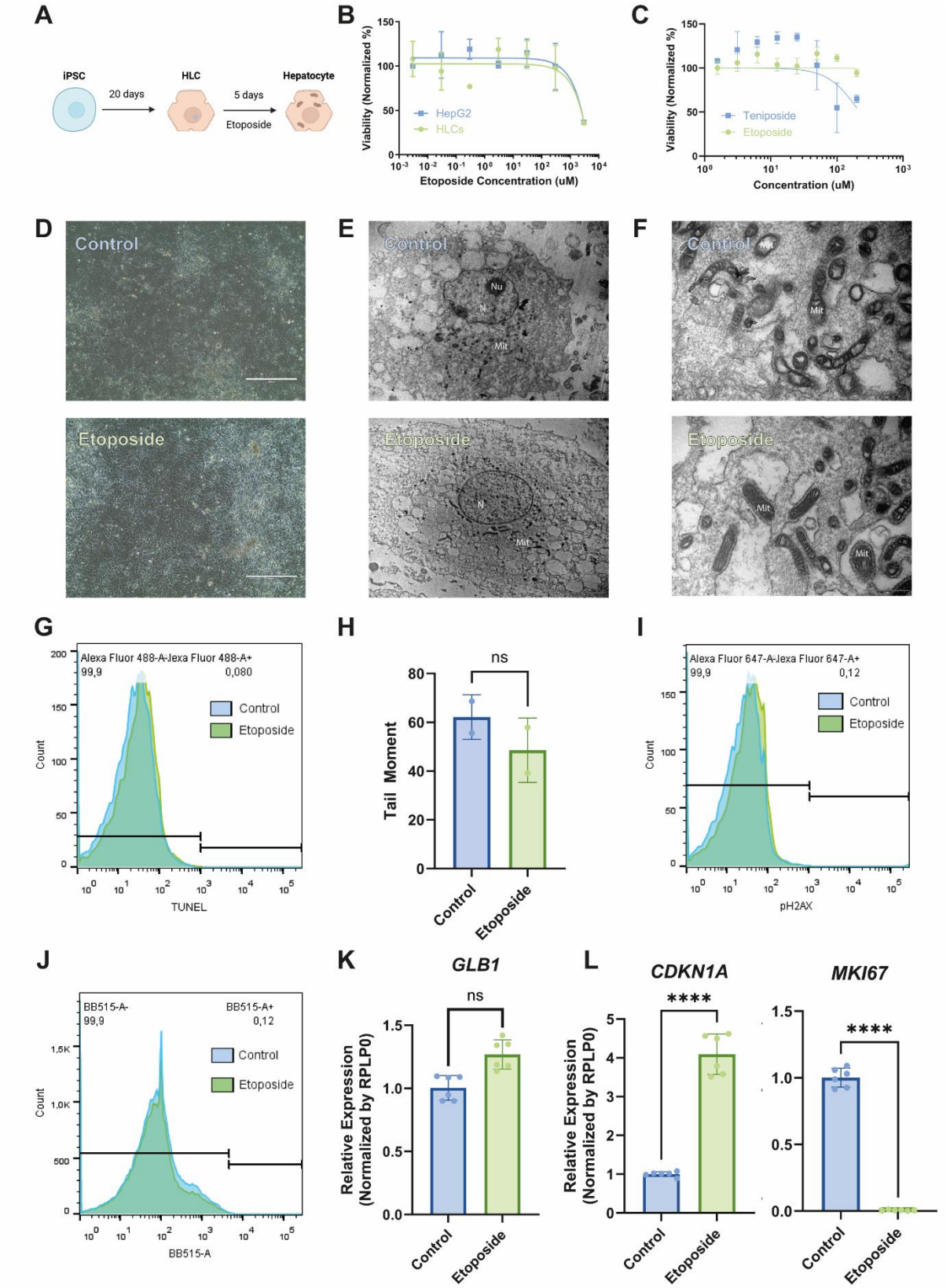
Fig. 4: Phosphoproteomic analysis of RCM-1- and etoposide-treated HLCs. A) Schematic of RCM-1 treatment of HLCs (Created using BioRender.com). **B**) Cell viability assay of HLCs with different concentrations of RCM-1 to determine toxic doses. **C**) Immunostaining for

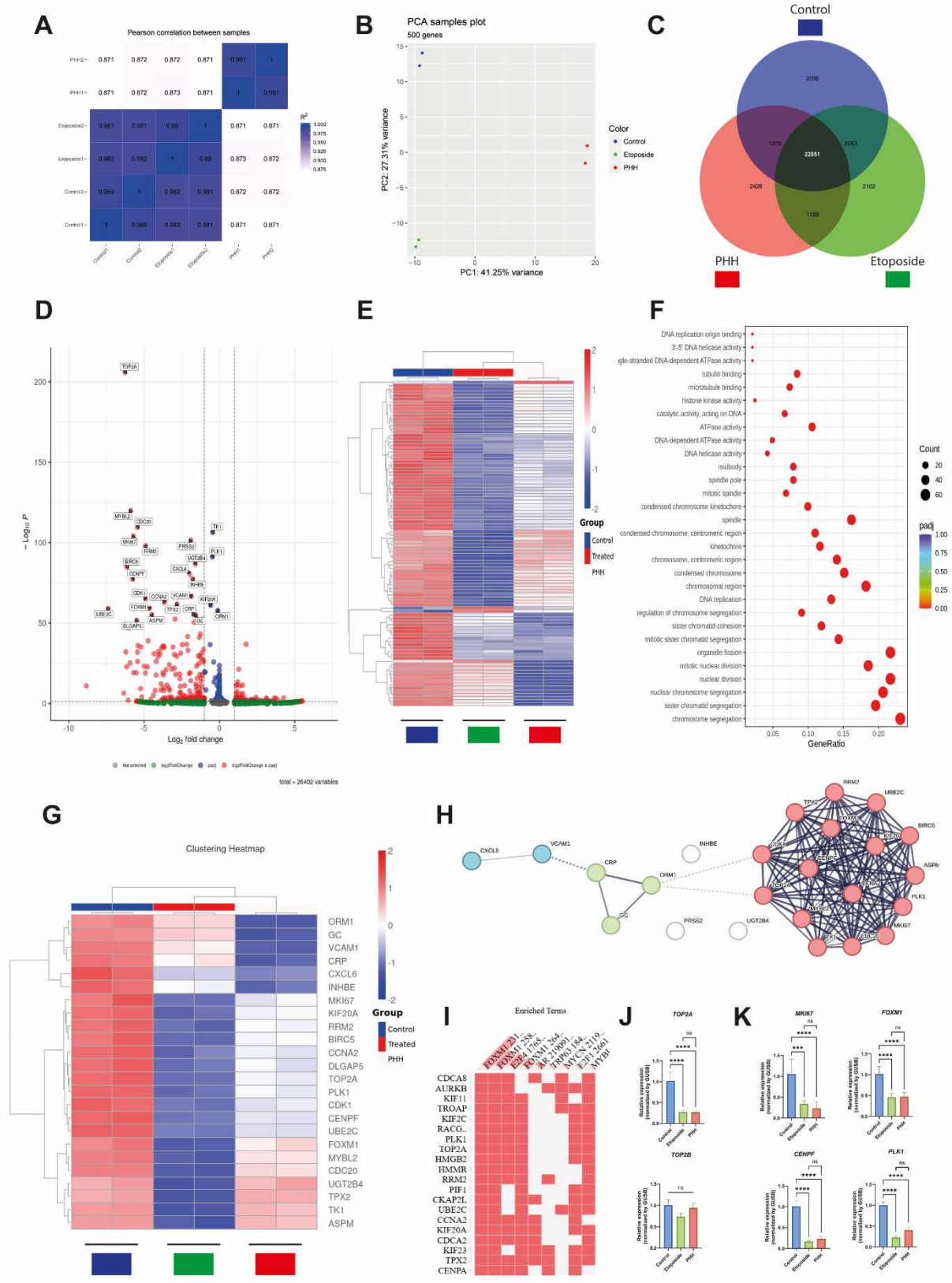
FOXM1 or phosphorylated Thr600 FOXM1 (pFOXM1) (Red) and DAPI (Blue) (scale bar = 300 μm). **D-E**) RT-qPCR of *TOP2A*, *TOP2B*, *FOXM1*, and *MKI67* (**D**); or *ALB*, *AFP*, *HNF4A*, and *CTNNB1* (**E**) of control, etoposide- and RCM-1-treated HLCs. **F**) Principal component analysis (PCA) on total identified peptides (21,353), adjusted for 500 features. **G**) Heatmap of the top 100 z-scored differentially abundant proteins between all samples. The colour represents the average abundance level of each protein. **H**) Volcano plot of differentially abundant proteins between RCM-1-treated and control HLCs (|log2(FoldChange)| >= 1 & FDR adjusted p-value <= 0.05)**. I**) ChEA analysis of the top 100 differentially abundant proteins between RCM-1-treated and control HLCs. The color and length of the bars indicate the combined ranked p-value and odds ratio. **J**) Expression2Kinases (X2K) analysis of the top 100 differentially abundant proteins between RCM-1-treated and control HLCs. The circle size indicates the number of differentially abundant targets of each transcription factor or kinase. **K**) Representative western blotting gels for ALB, AFP, TOP2A, CTNNB1, YAP/TAZ, SMAD1, and GAPDH. Blue, control HLCs; Green, etoposide-treated HLCs; Orange, RCM-1-treated HLCs. In B, C, D, E, and K, $n = 2$ biological replicates and 3 independent experiments. In F, G, and H, $n = 3$ biological replicates. In B, D, E, and K, data is mean ± SD. In D, E, and K, one-way ANOVA with multiple comparisons and Tukey's correction ($p<0.05$).

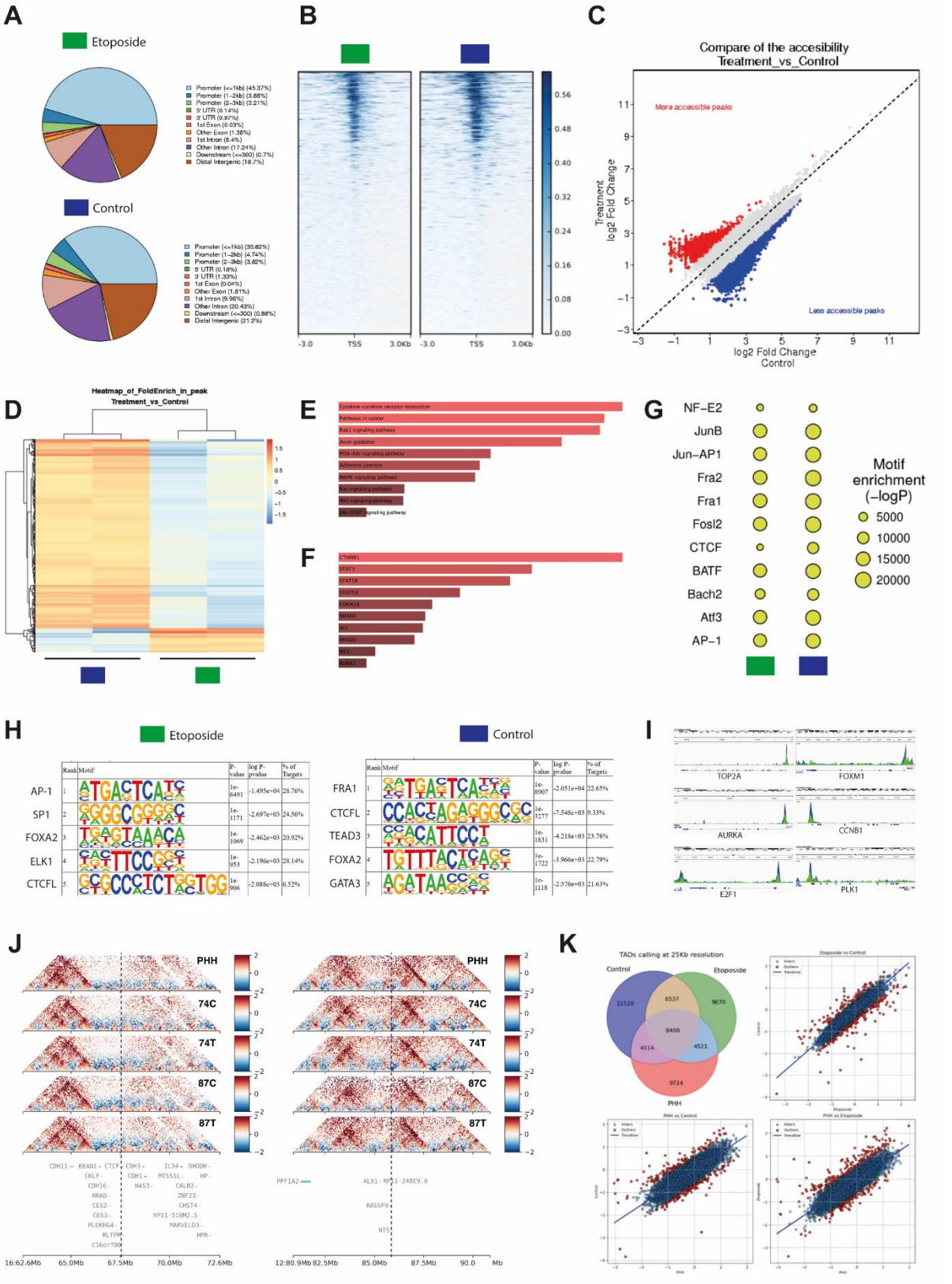
Fig. 5: FOXM1 inhibition promotes metabolic maturation and polyploidization of HLCs. **A**) Representative flow cytometry plots of the width versus height of the 535 channel (PI). Mononucleated diploid (2n), mononucleated tetraploid (4n), binucleated tetraploid (2n+2n), and binucleated octoploid (4n+4n) HLCs are shown. **B-E)** ELISA analysis of secreted CYP1A2 and CYP2B6 activity (**B**); secreted cholesterol and triglyceride (**C**); secreted alanine aminotransferase (ALT) and aspartate aminotransferase (AST) activity (**D**); and secreted

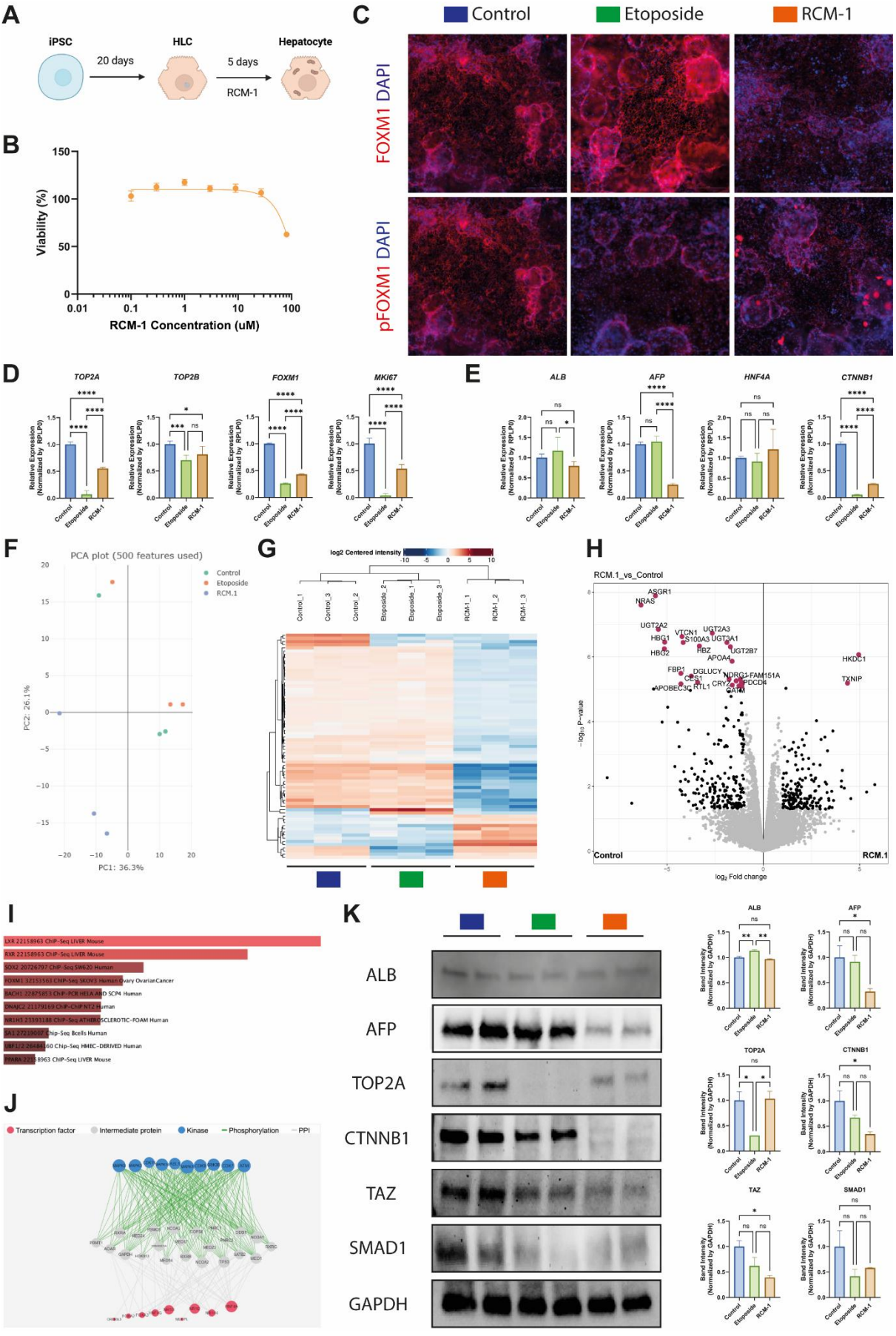
albumin (ALB) and alpha-fetoprotein (AFP) (**E**). **F**) Representative western blotting gels for ALB, AFP, CTNNB1, ERK1/2, and GAPDH. Blue, control HLCs; Green, etoposide-treated HLCs; Orange, RCM-1-treated HLCs. **G**) Schematic summary for the effects of FOXM1 and TOP2A inhibition in HLCs. Green arrow, activation; Red bar, inhibition (Created using BioRender.com). In every experiment, n = 2 biological replicates and 3 independent experiments. In all experiments, data is mean ± SD. In all experiments, one-way ANOVA with multiple comparisons and Tukey's correction ($p<0.05$).

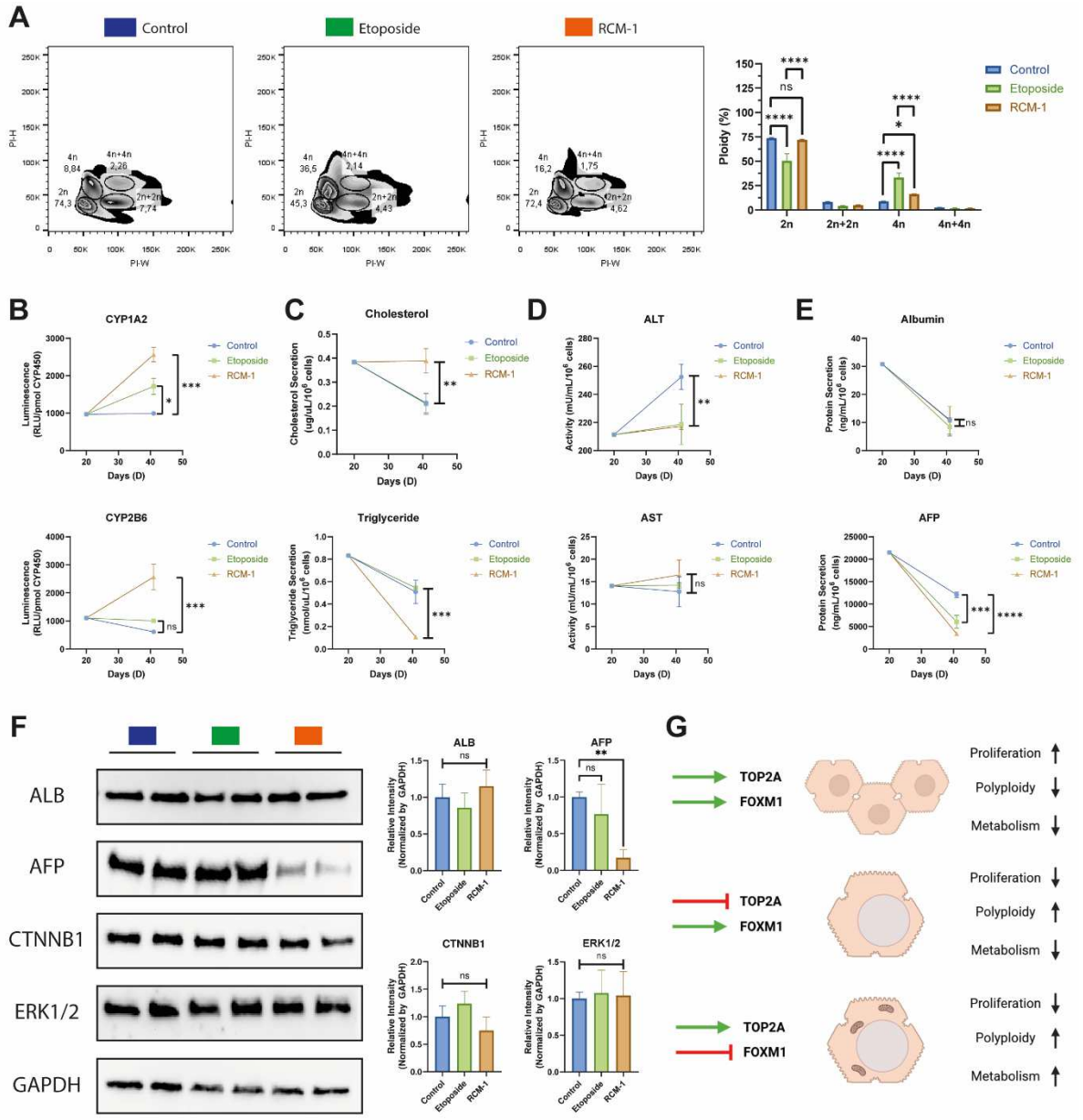
FIGURES


A
iPSC
20 days
HLC
5 days
Etoposide
Hepatocyte
B
Viability (Normalized %)
HepG2
HLCs
Etoposide Concentration (uM)
C
Viability (Normalized %)
Teniposide
Etoposide
Concentration (uM)
D
Control
Etoposide
E
Control
Nu
N
Mit
Etoposide
N
Mit
F
Control
Mit
Mit
Etoposide
Mit
Mit
G
Alexa Fluor 488-A-Jexa Fluor 488-A+
99,9
0,080
Control
Etoposide
Count
TUNEL
H
ns
Tail Moment
Control
Etoposide
I
Alexa Fluor 647-A-Jexa Fluor 647-A+
99,9
0,12
Control
Etoposide
Count
pH2AX
J
BB515-A-
99,9
BB515-A+
0,12
Control
Etoposide
Count
BB515-A
K
GLB1
ns
Relative Expression (Normalized by RPLP0)
Control
Etoposide
L
CDKN1A
****
MKI67
****
Relative Expression (Normalized by RPLP0)
Control
Etoposide
Control
Etoposide


A
Pearson correlation between samples
B
PCA samples plot
500 genes
PC2: 27.31% variance
PC1: 41.25% variance
Color
Control
Etoposide
PHH
C
Control
PHH
Etoposide
2096
1203
2053
22851
2428
2102
1199
D
Log2 fold change
E
Group
Control
Treated
PHH
F
DNA replication origin binding
3'-5' DNA helicase activity
igle-stranded DNA-dependent ATPase activity
tubulin binding
microtubule binding
histone kinase activity
catalytic activity, acting on DNA
ATPase activity
DNA-dependent ATPase activity
DNA helicase activity
midbody
spindle pole
mitotic spindle
condensed chromosome kinetochore
spindle
condensed chromosome, centromeric region
kinetochore
chromosome, centromeric region
condensed chromosome
chromosomal region
DNA replication
regulation of chromosome segregation
sister chromatid cohesion
mitotic sister chromatid segregation
organelle fission
mitotic nuclear division
nuclear division
nuclear chromosome segregation
sister chromatid segregation
chromosome segregation
GeneRatio
Count
padj
G
Clustering Heatmap
ORM1
GC
VCAM1
CRP
CXCL6
INHBE
MKI67
KIF20A
RRM2
BIRC5
CCNA2
DLGAP5
TOP2A
PLK1
CDK1
CENPF
UBE2C
FOXM1
MYBL2
CDC20
UGT2B4
TPX2
TK1
ASPM
Group
Control
Treated
PHH
H
CXCL6
VCAM1
INHBE
CRP
ORM1
GC
PRSS2
UGT2B4
RRM2
UBE2C
TPX2
BIRC5
KIF20A
ASPM
PLK1
MKI67
TK1
I
Enriched Terms
FOXM1_231...
FOXM1_258...
E2F4_1765...
FOXM1_264...
AR_219091...
TRP63_184...
MYCN_2110...
E2F_2661...
MYBL...
CDCA8
AURKB
KIF11
TROAP
KIF2C
RACG...
PLK1
TOP2A
HMGB2
HMMR
RRM2
PIF1
CKAP2L
UBE2C
CCNA2
KIF20A
CDCA2
KIF23
TPX2
CENPA
J
TOP2A
TOP2B
K
MKI67
FOXM1
CENPF
PLK1
Relative expression (normalized by GUSB)
Control
Etoposide
PHH


A
Etoposide
Promoter (<=1kb) (45.37%)
Promoter (1-2kb) (3.88%)
Promoter (2-3kb) (3.21%)
5' UTR (0.14%)
3' UTR (0.97%)
1st Exon (0.03%)
Other Exon (1.38%)
1st Intron (8.4%)
Other Intron (17.24%)
Downstream (<=300) (0.7%)
Distal Intergenic (18.7%)
Control
Promoter (<=1kb) (35.82%)
Promoter (1-2kb) (4.74%)
Promoter (2-3kb) (3.82%)
5' UTR (0.18%)
3' UTR (1.33%)
1st Exon (0.04%)
Other Exon (1.81%)
1st Intron (9.98%)
Other Intron (20.43%)
Downstream (<=300) (0.88%)
Distal Intergenic (21.2%)
B
-3.0
TSS
3.0Kb
C
Compare of the accesibility
Treatment_vs_Control
More accessible peaks
Less accessible peaks
Treatment
log2 Fold Change
log2 Fold Change
Control
D
Heatmap_of_FoldEnrich_in_peak
Treatment_vs_Control
E
Cytokine-cytokine receptor interaction
Pathways in cancer
Rap1 signaling pathway
Axon guidance
PI3K-Akt signaling pathway
Adherens junction
MAPK signaling pathway
Ras signaling pathway
Wnt signaling pathway
JAK-STAT signaling pathway
F
CTNNB1
STAT1
STAT3
STAT5A
CDKN1B
SMAD2
SP1
SMAD3
NFE2
NR3C1
G
NF-E2
JunB
Jun-AP1
Fra2
Fra1
Fosl2
CTCF
BATF
Bach2
Atf3
AP-1
Motif enrichment (-logP)
5000
10000
15000
20000
H
Etoposide
Control
Rank
Motif
P-value
log P-pvalue
% of Targets
AP-1
SP1
FOXA2
ELK1
CTCFL
FRA1
CTCFL
TEAD3
FOXA2
GATA3
I
TOP2A
FOXM1
AURKA
CCNB1
E2F1
PLK1
J
PHH
74C
74T
87C
87T
16:62.6Mb
65.0Mb
67.5Mb
70.0Mb
72.6Mb
12:80.9Mb
82.5Mb
85.0Mb
87.5Mb
90.0
Mb
K
TADs calling at 25Kb resolution
Control
Etoposide
11528
6537
9670
8400
4314
4521
9724
PHH


A
iPSC
20 days
HLC
5 days
RCM-1
Hepatocyte
B
Viability (%)
RCM-1 Concentration (uM)
C
Control
Etoposide
RCM-1
FOXM1 DAPI
pFOXM1 DAPI
D
TOP2A
TOP2B
FOXM1
MKI67
Relative Expression (Normalized by RPLP0)
E
ALB
AFP
HNF4A
CTNNB1
F
PCA plot (500 features used)
PC1: 36.3%
PC2: 26.1%
G
log2 Centered intensity
H
RCM.1_vs_Control
Control
RCM.1
I
J
Transcription factor
Intermediate protein
Kinase
Phosphorylation
PPI
K
ALB
AFP
TOP2A
CTNNB1
TAZ
SMAD1
GAPDH
Band Intensity (Normalized by GAPDH)


A
Control
Etoposide
RCM-1
PI-H
PI-W
4n
8,84
4n+4n
2,26
2n
74,3
2n+2n
7,74
4n
36,5
4n+4n
2,14
2n
45,3
2n+2n
4,43
4n
16,2
4n+4n
1,75
2n
72,4
2n+2n
4,62
Ploidy (%)
2n
2n+2n
4n
4n+4n
B
CYP1A2
Luminescence (RLU/pmol CYP450)
Days (D)
C
Cholesterol
Cholesterol Secretion (ug/uL/10^6 cells)
D
ALT
Activity (mU/mL/10^6 cells)
E
Albumin
Protein Secretion (ng/mL/10^6 cells)
CYP2B6
Triglyceride
Triglyceride Secretion (nmol/uL/10^6 cells)
AST
AFP
F
ALB
AFP
CTNNB1
ERK1/2
GAPDH
Relative Intensity (Normalized by GAPDH)
G
TOP2A
FOXM1
Proliferation
Polyploidy
Metabolism

Supplementary Files

This is a list of supplementary files associated with this preprint. Click to download.

- SupplementaryMaterial.pdf